Antonie van Leeuwenhoek (2026) 119:95
https://doi.org/10.1007/s10482-026-02300-2

ORIGINAL PAPER

Morphological plasticity of endophytic *Chitinophaga pinensis*

Janine Liedtke · Frans Rodenburg · Chao Du · Le Zhang · Jos M. Raaijmakers · Gilles P. van Wezel · Ariane Briegel

Received: 16 September 2025 / Accepted: 30 March 2026 / Published online: 11 April 2026
© The Author(s) 2026

Abstract Environmental changes, whether due to climate change or human influences, compromise the resilience of plants to biotic and abiotic stresses, such as pathogens, drought and heat. Plant microbiota are known to promote plant resilience. To be able to harness the power of the plant microbiome we need to identify microbiota with health-promoting properties. Recent studies have demonstrated that the bacterium *Chitinophaga pinensis* enhances plant health and increases resistance to fungal infections. Here, we show that *C. pinensis* exhibits an unusually high morphological plasticity, switching between a filamentous and a spherical cell state, each of which is characterized by a distinct transcriptional profile. Despite these transcriptional differences, spherical cells remained metabolically active and replicating, while lacking structural characteristics typically associated with dormant states. Furthermore, the spherical cell morphology of *C. pinensis* facilitates hitchhiking behaviour and motility via surfactin cheating, potentially influencing its dispersal and interactions within the plant microbiome. To investigate the structural dynamics and transcriptional adaptation of this plant endophyte, we applied a combination of microscopy and culture-based techniques. Taken together, our study provides new insights into the morphological flexibility and transcriptional regulation of the plant-beneficial *C. pinensis*.

Keywords *Chitinophaga pinensis* · Endophytes · Morphological plasticity · Hitchhiking

Supplementary Information The online version contains supplementary material available at https://doi.org/10.1007/s10482-026-02300-2.

J. Liedtke · F. Rodenburg · C. Du · L. Zhang · J. M. Raaijmakers · G. P. van Wezel · A. Briegel (✉)
Molecular Biotechnology, Institute of Biology, Leiden University, Sylviusweg 72, 2333BE Leiden, The Netherlands
e-mail: ariane.briegel@pasteur.fr

J. M. Raaijmakers
Department of Microbial Ecology, Netherlands Institute of Ecology (NIOO-KNAW), Wageningen, Netherlands

A. Briegel
Integrative Structural Cell Biology Unit, CNRS UMR 3528, Institute Pasteur, 75724 Paris, France

Introduction

Modern agriculture increasingly faces challenges due to climate change and a growing world population. Therefore, new measures and innovative strategies must be developed to conserve resources and minimize losses to ensure a sustainable future.

One of these strategies is to understand and utilize the natural defence and resistance mechanisms of plants. Numerous studies have already shown that the plant microbiota plays a decisive role in this context (reviewed in ref. Trivedi et al. 2020; Pan et al. 2023; Spooren et al. 2024)). Plants and their associated

microbiota are often referred to as a holobiont, as they engage in complex symbiotic interactions and have an evolutionary history as a community (reviewed in ref. (Vandenkoornhuyse et al. 2015)). Among the most abundant phyla within the plant microbiota, the phylum Bacteroidetes stands out as it contains numerous symbiotic strains associated with various hosts (Pérez-Jaramillo et al. 2018; Hildebrand et al. 2021).These microorganisms can enhance host fitness either directly by promoting plant health or indirectly by supporting other members of the microbiota. Those that colonize plant tissue without causing harm or negatively affecting the host are known as endophytes. Recent studies have shown that the endophytic strains *Flavobacterium anhuiense* and *Chitinophaga pinensis* contribute to plant health and improve stress tolerance (Carrión et al. 2019). The diversity of the plant-associated microbiota reflects a range of strategies that can enhance plant resilience. One such strategy is the "cry-for-help" response, in which plants actively recruit beneficial microbes by releasing root exudates in response to environmental stress. The composition of these exudates varies depending on the stress conditions, which leads to a specific metabolic adaptation of the bacteria already residing in the microbiota and stimulates the production of secondary metabolites (Rolfe et al. 2019; Liu et al. 2021, 2024; Spooren et al. 2024). However, effectiveness of induced stress tolerance depends on the microbiota composition, and missing key members can decrease the response effect (Salas-González et al. 2021). This effect is even more pronounced during activated defence mechanisms in the presence of plant pathogens (Matsumoto et al. 2021; Liu et al. 2024). In order to optimize the composition of the microbiota to protect plants naturally, it is important to identify key microbiome members and understand the factors involved in their recruitment.

As mentioned above, plants excrete root exudates to actively recruit and shape their microbiota according to their needs (Liu et al. 2021). These exudates contain diverse compounds, including sugars, amino acids, enzymes, fatty acids and polyphenols such as flavonoids (Vives-Peris et al. 2020). To successfully colonize the rhizo- and endosphere, microbes must be able to detect and respond to those signals. Many motile bacteria achieve this through chemotaxis, allowing them to sense and move along chemical gradients via chemosensory pathways that regulate flagellar motors (Briegel et al. 2014; Yang and Briegel 2020). Depending on their structural adaptations, bacteria utilize different motility strategies, including flagella-driven swimming and swarming or gliding motility, which relies on surface adhesins (Shrivastava and Berg 2015; Mattingly et al. 2018). However, some bacteria do not possess chemotaxis arrays or motility mechanisms. This raises the question of how these strains reach the plant and establish themselves within the microbiome. Previous research demonstrated that non-motile spores of endophytic *Streptomyces* can be transported by motile bacteria, a process known as hitchhiking (Muok et al. 2021). Hitchhiking allows non-motile bacteria to benefit from chemotactic movements without expending their own energy, potentially providing ecological advantages in host colonization. As proposed by Muok et al. (2021) (Muok et al. 2021) and Seymour (2024) (Seymour et al. 2024), hitchhiking can also yield in long-term benefits for bacterial communities, facilitating movements through barriers and promoting metabolic exchange.

Here, we focus on *Chitinophaga pinensis*, which was recently identified as an important member of the plant microbiota particularly regarding pathogen resistance and stress tolerance (Carrión et al. 2019). Originally isolated from pine litter, *C. pinensis* is a Gram-negative bacterium found in the endosphere of various plants, including crops (Carrión et al. 2019). It is known for its ability to degrade complex polysaccharides such as chitin and produce a variety of biologically active molecules, highlighting its potential value for agriculture and industrial applications (Brinkmann et al. 2022). Furthermore, previous studies have reported that *C. pinensis* forms so-called myxospores or microcysts, which have been hypothesized to represent a resting stage similar to bacterial spores (Sangkhobol and Skerman 1981; Reichenbach 1992; Glavina Del Rio et al. 2010). However, these structures have primarily been characterized based on their spherical morphology under the light microscope, and their metabolic state remained unclear. While most research on *C. pinensis* focused on its metabolic capabilities alone, in this study we investigated the ultrastructural morphology of cells as well as their interactions within the holobiont using a combination of microbiological assays, cryo-electron microscopy and transcriptomics. In particular, we aimed to gain insight into whether the morphology

of *C. pinensis* depends on the growth conditions, and see how this correlates to the strain´s ability to interact with plant tissue. Additionally, we aimed to determine whether these interactions are solely based on chemical signals or if physical structures, such as outer membrane vesicles (Kaplan et al. 2021), play a role in the communication with the plant. Notably, the *C. pinensis* strain studied by Carrión (2019) (Carrión et al. 2019) is neither motile nor equipped with chemotaxis arrays, which raises questions about its recruitment and ecological role within the holobiont. Finally, we investigated how these characteristics of *C. pinensis* contribute to its ecological function and potential impact on the dynamics of the plant microbiome.

Results

Chitinophaga pinensis shows two distinct cell morphologies

To gain a better understanding of the general morphology of *C. pinensis* over time, we investigated the cell culture at different incubation times by light microscopy. In fresh cultures up to 20h of growth, the cells are filamentous and can reach lengths of up to 40 µm, as described previously (Sangkhobol and Skerman 1981). Intriguingly, between 20h and 40h of growth, the morphology of *C. pinensis* dramatically transformed from several µm long filamentous cells to small spherical cells with a diameter of 600–700 nm (Fig. 1A). When transferred to fresh media with a lower cell density, the spherical cells reverted to the filamentous cell state (Online Resource 1). To gain a more detailed insight into these two cell morphologies, we used cryo-electron tomography (cryo-ET). Both cell types were enclosed by a typical Gram-negative cell envelope, enclosing a typical cytoplasm filled with evenly distributed ribosomes and other cellular content. Neither cell type resembled previously described spores or cysts, such as for example the presence of a thicker protective cell envelope (Fig. 1A).

To better visualize the morphological switching of *C. pinensis* from filamentous to spherical growth, we aimed to introduce GFP into the bacterium. The GFP labelling was designed to enable live-cell imaging and precise tracking of morphological changes, particularly since the spherical cells are very small (600–700 nm), making them difficult to keep in focus and distinguish from other particles or debris under the microscope. Therefore, the gene encoding GFP-mut3, under the control of its native *gap* promoter, was cloned into pCP23 (details in Materials and Methods), a shuttle vector between *Flavobacteria* and *E. coli*. The resulting construct, pGWS1802, was successfully introduced via electroporation. However, the plasmid was not stably maintained: green fluorescence diminished with each subsequent bacterial generation. This suggests that the plasmid failed to replicate in *C. pinensis*, most likely due to incompatibility of the repB replication origin on pCP23, which is optimized for Flavobacteria and does not function effectively in this species.

Resistance profiles of cell morphologies to physical and chemical stressors

The small spherical cells observed after prolonged growth were consistent with previous reports, which described them as microcysts or spores. However, our cryo-ET results revealed that the small spherical cells forms do not have a typical spore morphology, such as a thickened cell envelope and tightly packed cytoplasm content. Therefore, we wondered whether the two cell morphologies exhibit distinct responses to various physical and chemical stress factors. Both cell morphologies exhibited similar resilience to the following stress factors: UV light irradiation for 10 min, heat stress at 60 °C and sonication for up to 5 min. Both cell morphologies of *C. pinensis* survived after desiccation and could be revived by plating on fresh medium. Light microscopic examination of the desiccated *C. pinensis* cells revealed small spherical cells, independent of their initial morphology. Further chemical stress tests showed slight differences in resistance behaviour of the two cell morphologies in response to changes in the pH and in the presence of up to 0.2% ethanol (Fig. 1B). However, in the presence of 2% ethanol, both cell morphologies exhibited reduced growth. Neither cell morphology of *C. pinensis* grew in SDS-containing (0.02–2%) media.

Overall, the spherical morphology exhibited higher OD_{600}-based carrying capacity and a slightly shorter doubling time compared to the filamentous cell morphology (Fig. 1B). Nevertheless, the differences in

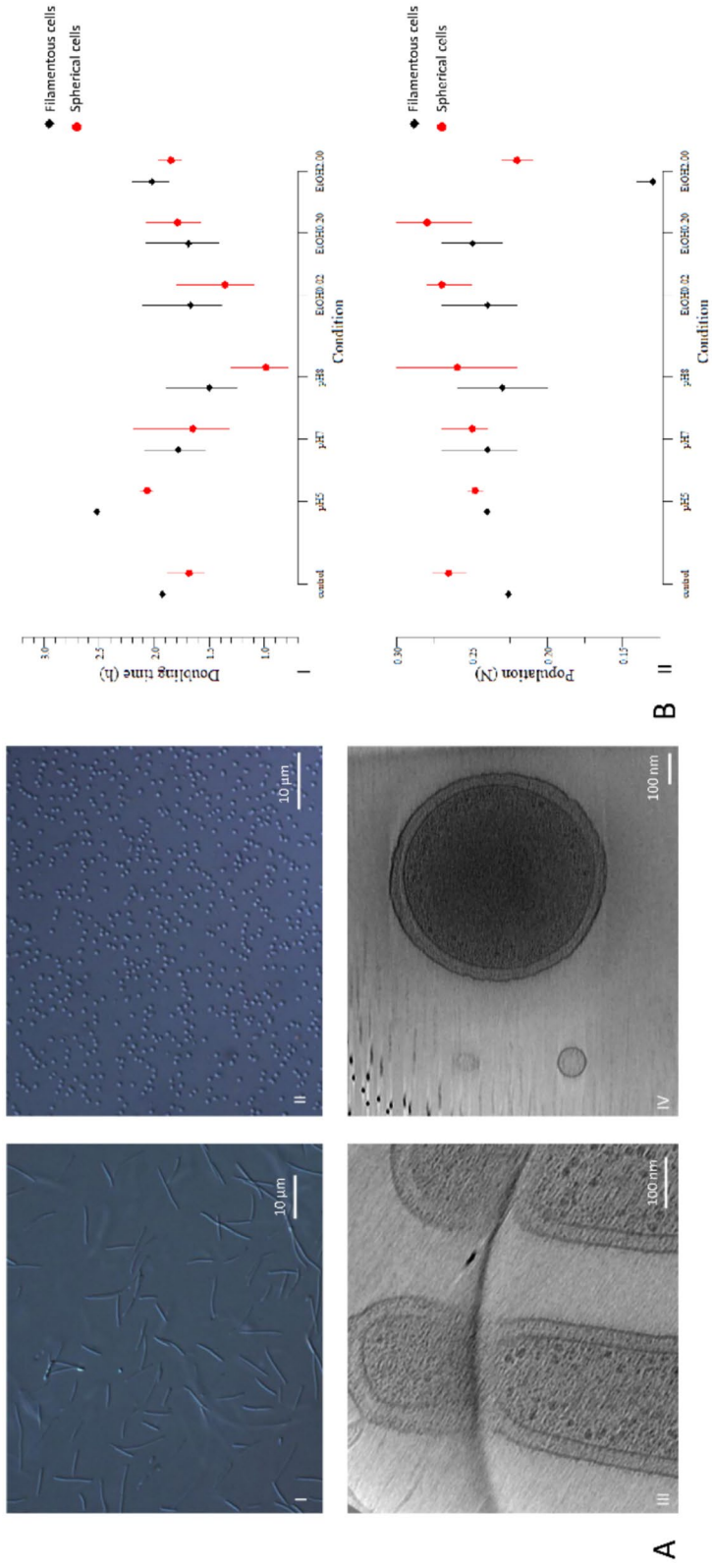

Fig. 1 Morphological plasticity and stress resistance for the *C. pinensis* morphotypes. **A** Cells were imaged by light microscopy (AI–II; scale bar 10 µm) and cryo-electron tomography (AIII–IV; scale bar 100 nm). (AI) Long filamentous cells after 20h and small spherical cell shape after 40h of incubation. **B** Chemical stressor assay: Resistance behaviour of both morphologies was tested in 0.1 × TSB medium supplemented with increasing ethanol concentrations or altered pH. Measured were the change of OD_{600} over 20h and displayed are the calculated growth parameters: doubling time (BI) and carrying capacity (BII) based on fitted growth curves with a confidence interval of 95%. (N = 3)

the resistance profiles between the two morphologies were marginal.

Next, we investigated whether the decrease in cell size and the formation of small spherical cells represented a stress reaction. For this purpose, growth in the presence of salt (0.5–2%) or chloramphenicol (12.5–100 µg/ml) was analysed. When cells with a filamentous phenotype were exposed to higher salinity and chloramphenicol concentrations, a decrease in cell length was observed (Online Resource 2). With increasing salt and chloramphenicol concentrations, the spherical cells tended to dominate the culture faster compared to the control conditions (Online Resource 2). Regardless of the salt and chloramphenicol concentration in the medium, spherical cells appeared in all cultures after 2 days of incubation.

Transcriptomic analysis of 20h and 40h cultures

Spherical cells were previously assumed to be dormant spores. However, the cryo-EM and resistance assays presented here revealed no structural or physiological features typically associated with dormancy. To assess the changes in transcriptional patterns between the two time points and corresponding culture types, we performed transcriptomic analysis on RNA obtained from cultures harvested after 20h and 40h of growth. Microscopic inspection before RNA extraction confirmed that the 20h and 40h samples predominantly displayed filamentous and spherical morphologies, respectively. Although the presence of rare cells of the alternate morphology cannot be fully excluded, the samples were clearly dominated by the expected cell type, making it unlikely that residual filamentous cells account for the observed transcriptional profiles. All cultures were grown under identical conditions (1.0×TSB, 25 °C, 250 rpm) (Online Resource 1). Growth curves shown in Online Resource 3 were obtained after harvesting cells at 20h and 40h, adjusting them to identical OD_{600} values, and reinoculating them into fresh medium. At both sampling points (20h and 40h), the OD_{600} of the shake-flask cultures from which the samples were taken was still increasing, indicating that the cultures had not yet reached a fully stationary state. Attempts to quantify growth by colony forming unit (CFU) enumeration were not successful, because early colonies remained too small for reliable detection and later colony merging prevented accurate counting.

Principal component analysis (PCA) showed a clear transcriptional distinction between the two time points (Online Resource 4). Differentially expressed genes (DEGs) were defined as showing a fold change of ≥ 2 (FC ≥ 2) and an adjusted *p*-value (padj) of 0.05. Based on these criteria, 691 genes were upregulated and 615 downregulated in the 40-h samples compared to the 20-h samples of a total of 6094 genes (Online Resource 5). The lists of up-, down-regulated DEGs and all DEGs were subjected to KEGG pathway enrichment analysis (Table 1). Genes downregulated at 40-h were significantly enriched for ribosomal components (cpi03010), and amino acid biosynthesis genes (cpi01230) were strongly underrepresented among the upregulated genes. Additionally, genes involved in fructose and mannose metabolism (cpi00051) and fatty acid biosynthesis (cpi00061) were predominantly downregulated. Within the fatty acid biosynthesis pathway, most of the identified genes

Table 1 KEGG pathway enrichment analysis of differentially expressed genes (DEGs)

DEG list	KEGG	Pathway	Total	List	PW total	PW DEGs	log2EF	FDR
All	cpi01100	Metabolic pathways	6094	1306	647	105	−0.40	5.56e−3
All	cpi03010	Translation	6094	1306	57	46	1.91	1.51e−19
Down	cpi00051	Fructose metabolism	6094	615	20	9	2.16	3.24e−3
Down	cpi00061	Fatty acid synthesis	6094	615	25	9	9	1.55e−2
Down	cpi03010	Translation	6094	615	57	46	3.00	2.38e−34
Up	cpi01100	Metabolic pathways	6094	691	647	44	−0.74	8.76e−4
Up	cpi01230	Amino acid biosynthesis	6094	691	124	1	−3.81	5.42e−4

Columns indicate total genes in the genome (Total), DEGs per list (List), KEGG pathway size (PW total), number of DEGs in the pathway (PW DEGs), log_2 enrichment factor (log_2EF), and Benjamini–Hochberg FDR (FDR).

(19 out of 25) showed reduced expression, including 9 DEGs, indicating a broad transcriptional shift in this pathway.

Despite the observed downregulation of genes involved in translation and biosynthesis processes at 40-h, growth measurements under control conditions showed comparable growth dynamics after reinoculation for both time points. The doubling time was 1.53h at 20-h ($\mu = 0.45\ h^{-1}$, 95% CI: 1.32–1.83), and 1.62h at 40-h ($\mu = 0.43\ h^{-1}$, 95% CI: 1.39–1.94) and the confidence intervals overlapped. A Welch t test comparing the growth parameters of the 20h and 40h controls showed no significant difference ($p = 0.350$; 95% CI: -0.359–0.834).

Morphological variation under different culture conditions

Next, we sought to determine whether specific culture conditions influence the extent or speed of the observed morphological changes. For this, we systematically varied (i) cell density ($OD_{600} = 0.2$ and 0.5), (ii) nutrient content, and (iii) the presence of components in conditioned media, using five different media: fresh medium (0.1 × TSB; FM), spent medium from filamentous cells (LM), spent medium from spherical cells (SM), SM supplemented with fresh medium (SMT), and phosphate-buffered saline (PBS; B). As these factors are interrelated, they were tested by adjusting their concentrations in the media.

Across FM, LM and SMT media, the general pattern was a decrease in cell length of approximately 29% for filamentous cells and an increase of about 74% for spherical cells over the measured time (Fig. 2).

For both morphologies, measurable changes in cell length were observed after 3h compared to the initial values, and density-related differences became apparent. After a total of 6h, these differences decreased, and the cell lengths showed a trend towards convergence within each cell morphology (Fig. 2).

The influence of cell density was more pronounced in filamentous cells than in spherical cells. In spherical cells, both densities led to a similar increase in length, differing primarily in the speed of increase. In contrast, filamentous cells showed different patterns depending on the initial density; at high density (0.5), cell length decreased continuously by approx. 32% after 6h, while at low density (0.2), the cell length initially decreased by 45% after 3h, followed by an increase of approx. 27% after 6h. This general pattern was consistent across FM, LM and SMT media. Deviations from this general pattern were observed in B and SM media, whereby in medium B at higher cell density (0.5), filamentous cells increased in length by approximately 6% over time (Fig. 2B), while in SM media at lower cell density (0.2), filamentous cells continued to decrease in length after 6 h (approx. 48%) (Fig. 2C).

During the experiment, we assumed that the nutrient content of the media decreased in the following order, from the highest to the lowest content: SMT > FM > LM > SM > B. Whereby medium B was assumed to contain neither nutrients nor potential extracellular factors. We also presumed that LM contained extracellular factors from filamentous cells, while SM and SMT were assumed to contain extracellular factors from spherical cells.

Overall, changes in cell length were observed in both cell morphologies under all conditions tested. Comprehensive details and individual diagrams for each condition are provided in the supplementary materials (Online Resource 6).

Chitinophaga pinensis spherical cells are dispersed by *B. subtilis*

Based on our observation that *C. pinensis* is non-motile under the condition tested (Online Resource 7) and exhibits morphological plasticity, we next investigated whether the spherical cells could provide an adaptive advantage, particularly in terms of their potential to hitchhike on motile bacteria.

Here, we repeated the hitchhiking assay according to Muok et al. (2021) (Muok et al. 2021) in order to determine the hitchhiking ability of the two cell morphologies of *C. pinensis*. For this purpose, spherical cells of *C. pinensis* were isolated and placed on semi-solid media plate over *B. subtilis*. The hitchhiking behaviour of *C. pinensis* cells was assessed by observing their spreading indicated by the yellow-orange colonies.

As shown in Fig. 3A(III), when spherical cells were added, the yellow colonies spread across the plate.

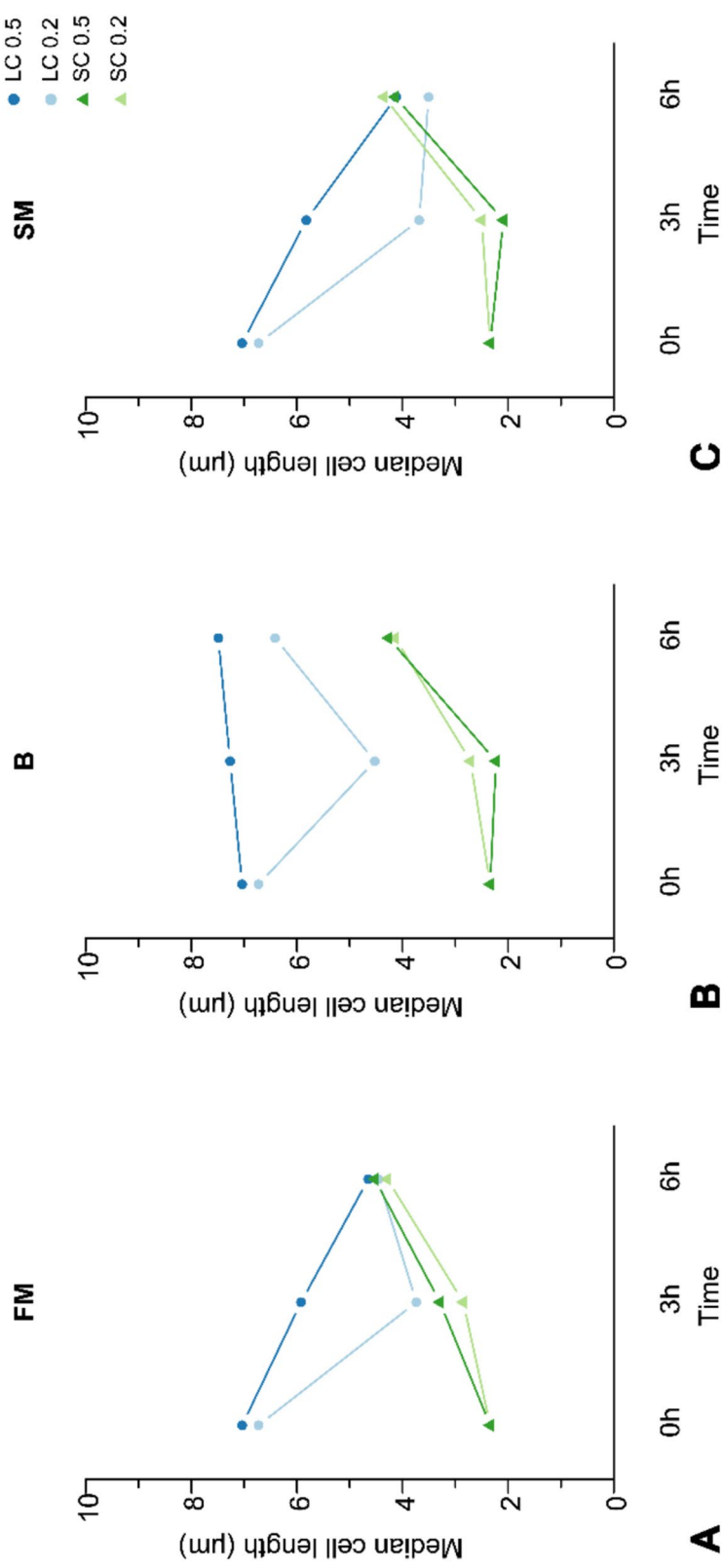

Fig. 2 Trigger test of morphological change. Observed pattern of change in cell morphology under different growth conditions (N = 3). Shown is the determined median of cell length for each cell morphology at the cell densities of $OD_{600} = 0.2$ and 0.5 at the measured time points: 0, 3, and 6h. Corresponding distributions are shown in Online Resource 6. **A** Illustration of the predominant pattern of cell length change observed in the different media, here using fresh medium (FM) as an example. Deviating patterns were observed in PBS (B) and spent medium from spherical cells (SM) for filamentous cells. **B** Illustration of the pattern of filamentous cells with an initial $OD_{600} = 0.5$ in medium B. **C** Deviating pattern of filamentous cells at an initial cell density of $OD_{600} = 0.2$ in medium SM. The median cell length is given in µm. Media: FM = fresh 0.1 × TSB; LM = spent medium from filamentous cells; SM = spent medium from spherical cells; SMT = SM supplemented with fresh medium; B = PBS. These media were used to test the influence of nutrients and conditioned supernatants on cell-length dynamics

To understand the nature of the hitchhiking behaviour, we tested the ability of *C. pinensis* to hitchhike in the presence of *B. subtilis* mutants that were impeded in their movements either by inhibition of surfactin production (Δ*espH srfAA*::mls), suppression of flagellar motility (Δ*motAB*) or absence of flagella (Δ*hag*). In addition, a laboratory strain of *B. subtilis* (DK605) that had lost its swarming ability (Muok et al. 2021) was included in this study. The test revealed that the hitchhiking behaviour of *C. pinensis* is independent of flagellar movement and the presence of flagella. While the spherical cells can be dispersed by swarming and sliding motility of *B. subtilis*, they cannot be dispersed by a *B. subtilis* mutant (Δ*espH srfAA*::mls) that is limited to swimming motility and unable to produce surfactin. A surfactin cheating assay demonstrated that the spherical cells of *C. pinensis* follow surfactin dispersal in and on media surface (Fig. 3B(I)).

Next, we tested whether the spherical cells of *C. pinensis* follow the surfactin spreading in the presence of *B. subtilis* cells, assuming that the surfactin produced by *B. subtilis* cells is distributed over the entire plate due to their movement. Despite the presence of surfactant on the entire plate, *C. pinensis* cells only spread along the movement of *B. subtilis* (Fig. 3B(II)). When the spherical cells were placed between two *B. subtilis* inoculation sites, the *C. pinensis* colonies remained between them. Although the spherical cells of *C. pinensis* can cheat using *B. subtilis* surfactin, they cannot spread in the opposite direction of *B. subtilis* movement (Fig. 3B(II)).

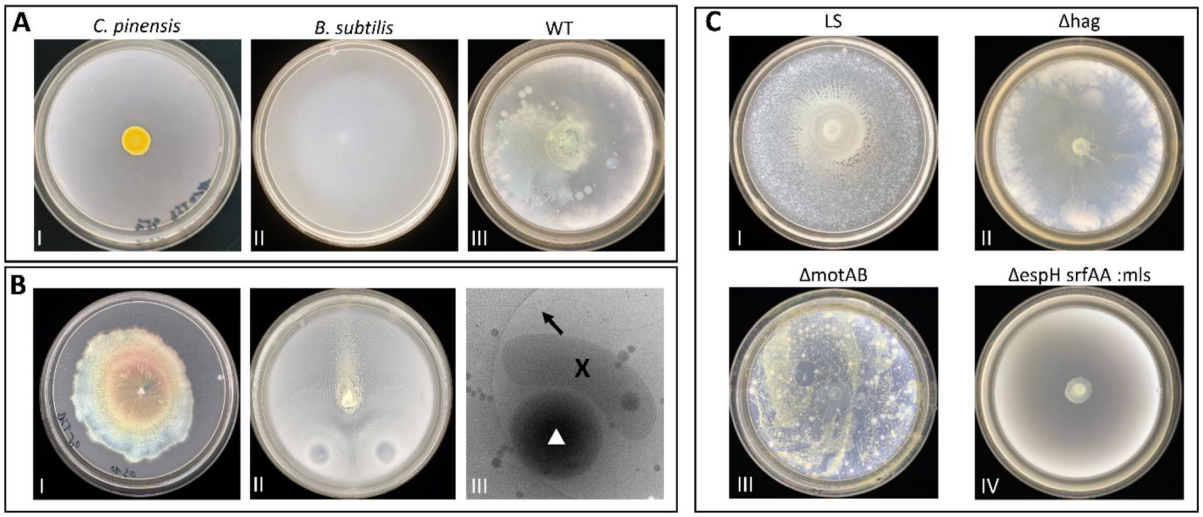

Fig. 3 Motility and hitchhiking interaction between *Chitinophaga pinensis* and *Bacillus subtilis.* **A** Motility assay and co-culture-dependent dispersal. (AI) *C. pinensis* grown alone did not display motility under the tested conditions and its yellow colony remained at the point of inoculation. (AII) Motile *B. subtilis* wild-type strain (WT; NCIB3610) grown alone exhibited surface spreading. (AIII) When spherical *C. pinensis* cells were combined with a motile *B. subtilis* wild-type strain (WT; NCIB3610) (AII), yellow colonies spread over the plate. **B** Surfactin exploitation and collective crowd movement. (BI) Further tests showed that *C. pinensis* can exploit externally supplied surfactin derived from *B. subtilis*. (BII) However, in the presence of *B. subtilis* and using initially spherical *C. pinensis* cells, the yellow colonies followed the collective crowd movement of the expanding *B. subtilis* colonies. (BIII) Cryo-EM imaging revealed the interaction between the two organisms: a black arrow indicates *B. subtilis* flagella, black X-mark denotes *C. pinensis*, and white triangle indicates *B. subtilis*. **C** Hitchhiking assays with *B. subtilis* strains differing in motility. Hitchhiking assays using spherical *C. pinensis* cells were also performed with a *B. subtilis* laboratory strain (LS; DK605; CI) that has lost its swarming capability, as well as mutants with impaired motility, including a strain lacking flagella (Δ*hag*; CII), a strain defective in flagellar rotation (Δ*motAB*; CIII), and a surfactin-deficient strain (Δ*espH srfAA*\::mls; CIV). These assays revealed flagella-independent hitchhiking, whereas dispersal was not observed with swimming-only strains (CIV).

Discussion

C. pinensis has two morphologies with distinct transcriptional profiles

C. pinensis is described in the literature as a long filamentous bacterium that can produce small spherical bodies, often referred to as myxospores, microcysts or spores, and assumed to represent a dormant stage (Sangkhobol and Skerman 1981; Reichenbach 1992; Glavina Del Rio et al. 2010). Although these terms are frequently used, there is neither a clear definition nor a distinction between them (Sly et al. 1999). Dormancy is defined as an adaptive state of reduced metabolic activity and arrested growth that enhances survival under unfavourable conditions (McDonald et al. 2024). It is typically associated with structural and physiological adaptations such as thickened cell walls, condensed DNA, and enhanced resistance to environmental stressors (McDonald et al. 2024).

However, stress resistance assays and structural analysis suggest that morphological changes in *C. pinensis* do not follow the classical characteristics of dormancy-associated differentiation. Our transcriptomic analysis indicates a shift in gene expression patterns in spherical cells, suggesting a metabolic slow down, although cells continue to proliferate and maintain distinct transcriptional activity. Furthermore, there was no major difference in growth behaviour between cells harvested at 20h and 40h under the tested conditions (Online Resource 3).

It should be noted that OD_{600} measurements can be influenced by differences in cell morphology. For this reason, OD-based growth curves were interpreted only in a relative sense and always under identical measurement conditions. The growth trends observed across replicates were consistent for both sampling points. Although absolute growth rates cannot be inferred from OD_{600} values alone, the relative growth parameters obtained for the 20h and 40h culture were comparable across independent replicates, indicating that the estimated growth rates are robust within the constraints of this assay.

These results suggest that *C. pinensis* does not really enter a dormant phase but instead modulates its transcriptional profile at the molecular level as part of an adaptive response to changing nutrient availability and environmental conditions.

Morphological plasticity is a well-documented survival strategy among bacteria, enabling them to respond dynamically to environmental change. Some bacteria undergo sporulation under unfavourable condition, whereas others alter their morphological characteristics to optimize resource acquisition, evade predation, or adapt to fluctuating nutrient availability. *Escherichia coli*, for example, can undergo filamentation under stress to avoid predation or shrink size to minimize metabolic demands (Justice et al. 2006; Campey et al. 2024). In this context, the ability of *C. pinensis* to transition between morphologies may provide similar ecological advantages, contributing to its persistence in diverse environments. Beyond individual survival, morphological transitions can also play a role in microbial community dynamics and interactions with host organisms. Previous studies have shown that microbial morphology can influence biofilm formation, resource competition, and interspecies interactions within complex microbiomes (Justice et al. 2008; Rizzo et al. 2020; Karasz et al. 2022). However, as noted by Shah (2019) (Shah et al. 2019), the ecological consequences of morphological differentiation in bacteria remain underexplored. In the case of *C. pinensis*, the impact of its morphological states on its functional role within the plant microbiome remains unclear.

Relevance of morphological and transcriptional plasticity for host–microbiota interactions

Previous studies on morphological plasticity have primarily focused on stress responses, often overlooking concurrent metabolic changes (Ultee et al. 2019; Shah et al. 2019; Karasz et al. 2022). Consequently, the link between morphology and transcriptional changes beyond stress adaptation remains insufficiently explored. The observed morphological and transcriptional plasticity in *C. pinensis* challenges conventional assumptions, as filamentation is typically associated with stationary phase adaptation, where secondary metabolite production is prioritized over cell growth and occurs as a stress response (Xavier 2011). In this way, bacteria ensure that secondary metabolites are produced at low cost and with high benefit (Santamaria et al. 2022). In *C. pinensis*, however, filamentation during early growth coincides with increased transcription of genes annotated as secondary metabolism-related, when nutrients are

abundant and cell density is low. Filamentation is energetically costly and can reduce fitness and carrying capacity (Karasz et al. 2022; Santamaria et al. 2022), suggesting it must provide compensatory benefits in *C. pinensis*. Filamentation has been associated with several ecological advantages, including improved surface interactions, biofilm formation, competitive polymer degradation, nutrient acquisition in heterogeneous environments, and a possible intracellular spreading mechanism (Wucher et al. 2019; Nunan et al. 2020; Tran et al. 2022). The interplay between morphological and transcriptional plasticity in *C. pinensis* reflects a complex regulatory network within the holobiont, likely contributing to microbial stability and adaptation. However, further research is needed to determine whether these morphological transitions provide ecological advantages in competitive environments and how they influence plant–microbe interactions (Xavier 2011; Lyons and Kolter 2018).

Hidden trigger of recurrent morphological change

To identify triggers for morphological change beyond stress factors, three commonly described factors–nutrient availability, components present in conditioned media, and cell density–were tested (Weart et al. 2007; Rizzo et al. 2020). Since these factors co-occur, they could not be tested in isolation. Instead, their concentrations were varied, and the speed of morphological change was analysed. Despite these efforts, no clear trigger could be identified, suggesting a complex interplay of growth conditions and regulatory mechanisms. Previous studies have shown that triggers are only effective under certain conditions. If these conditions are not met, the cell's regulatory mechanisms intervene and prevent the response (Karasz et al. 2022). This could explain why the filamentous cells in SMT increased in size after six hours, whereas in SM, they continued to decrease (Online Resource 6). Both media are derived from spherical cells but differed in nutrient composition. Additionally, this effect was absent in filamentous cells at higher initial cell densities, which is a further indicator for a complex interplay of regulatory mechanisms.

Triggers may also be masked by secondary effects. It was suggested that high phosphate concentrations may trigger filamentation of *Paraburkholderia elongata* (Karasz et al. 2022). However, further analysis revealed that the actual trigger was magnesium deficiency, resulting from intracellular polyphosphate chelation. Similarly, our findings suggest that morphological changes in *C. pinensis* are linked to cell density. This is supported by observations that filamentous cells exhibited density-dependent differences in cell length dynamics, while spherical cells increased in size under all tested conditions (Online Resource 6). This may be due to dilution effects, as spherical cells were harvested from a high-density culture, potentially initiating morphological transitions.

Growth rate, rather than cell density alone, likely plays a key role in morphological changes as well (Weart et al. 2007; Xavier 2011; Tran et al. 2022). The metabolic sensor UDP-glucose has been shown to link carbon availability to growth rate by controlling FtsZ ring assembly, a key regulator of bacterial cell division (Weart et al. 2007; Xavier 2011; Tran et al. 2022). However, *C. pinensis* is genetically not readily tractable and despite extensive attempts we could not express FtsZ-GFP.

Spherical cells can hitchhike and potentially utilize chemotaxis of others

Although motility via the type IX secretion system (T9SS) is known in other *C. pinensis* strains (McBride and Zhu 2013), it could not be induced in the strain used in our experiments. This limitation led us to explore whether morphological plasticity provides alternative advantages beyond metabolic efficiency. Given their small size (600–700 nm), the spherical cells of *C. pinensis* could be transported by vascular pressure within plant tissue. However, their movement in soil remains unclear. Without chemotaxis genes, they may rely on other motile bacteria for translocation. Previous studies have shown that some non-motile bacteria exploit the motility of others for their dispersal. For example, the spores of *Streptomyces* can attach to the flagella of motile bacteria (Muok et al. 2021), while the coccoid cells of *Staphylococcus* attach directly to the cell body of swimming bacteria and can be passively translocated (Samad et al. 2017).

In our experiments, spherical cells of *C. pinensis* exhibited hitchhiking behaviour but unlike *Streptomyces* spores, this interaction was independent of carrier mobility and presence of flagella. Notably,

hitchhiking was observed on swarming plates but not on swimming plates indicating that surface conditions influence this interaction (Fig. 3C) (Li et al. 2021; Engelhardt et al. 2022). In addition, gliding, sliding, and swarming are classified as crowd movements, whereas swimming is an individual behaviour (Kearns 2010; Mattingly et al. 2018). Crowd movements are an energy-saving, protective and efficient translocation mechanism that optimizes the search for resources in a nutrient-heterogeneous environment such as soil (Ariel et al. 2015; Nunan et al. 2020; Engelhardt et al. 2022).

Microscopy imaging further supports that hitchhiking in *C. pinensis* is transient rather than a stable attachment, distinguishing it from *Streptomyces* spores. As observed in Fig. 3B(III), *C. pinensis* cells loosely associated with *B. subtilis* minicells, possibly via hydrophobic interactions. Notably, Fig. 3B(III) shows a small, rod-shaped *C. pinensis* cell in association with *B. subtilis*. Since spherical cells were used as inoculum, it cannot be ruled out that some cells elongated under the conditions of the hitchhiking assay. However, the extent to which this change promotes hitchhiking behaviour in *C. pinensis* remains unclear.

In dense bacterial communities, population often align in liquid–crystal-like arrangements, promoting collective movement (Meacock et al. 2021). Consistent with this, *C. pinensis* spherical cells moved with *B. subtilis* rather than dispersing independently, despite being capable of surfactin cheating. Cheating on public goods, such as surfactin, is a well-known strategy in cooperative communities (Xavier et al. 2011; Lyons and Kolter 2018). However, *B. subtilis* employ regulatory mechanisms to mitigate cheater exploitation (Lyons and Kolter 2018). Thus, while hitchhiking behaviour was observed, it remains unclear whether *C. pinensis* actively engages in this process or undergoes passive translocation driven by *B. subtilis* crowd movements. Resolving this distinction is essential for understanding bacterial dispersal mechanisms and plant root colonization.

Regardless of the exact mechanism underlying *C. pinensis* hitchhiking, this behaviour may represent an alternative mode of bacterial dispersal that allows non-motile bacteria to achieve spatial relocation in structured environments.

Each piece of knowledge contributes to unravelling and understanding the dynamic interaction within the host-microbiota. In addition, the question of the critical ratio of mobile and immobile bacteria that still allows community mobility should be answered. Considering that some bacteria are motile at low and others at high cell density, the question arises whether this contributes to the community remaining motile under different conditions. It would be also interesting to investigate the extent to which hitchhiking behaviour influences this movement, especially in the presence of plant roots. Some of these questions could potentially be explored in future studies using transparent soil and light-sheet fluorescence microscopy.

Conclusion

Climate change and pollution from conventional agriculture degrade resource quality and put additional stress on plants, weakening their resilience. Preserving the natural occurring plant-protective microbes in the plant microbiota can improve plant resilience and immunity. To understand the complex interactions between plants and their microbiota and within the microbiota, the key members must first be identified and then their interaction mechanism uncovered.

One such key member is *C. pinensis*, known for its plant-health-promoting characteristics, demonstrated significant morphological plasticity transitioning from a long filamentous to a small spherical cell shape, accompanied by distinct transcriptional changes. Despite this transition, the spherical cells do not exhibit dormancy-like traits such as structural differentiation, increased resistance, or arrested growth but remain reproductive. In addition, the transition into small spherical cells may facilitate flagella-independent translocation mediated by motile bacteria.

Further work is needed to uncover the triggering and control mechanisms of morphological and metabolic plasticity and their role in dynamic and complex interactions. In addition, it is crucial to investigate the extent to which translocation, whether by hitchhiking or crowd movement, contributes to colonization and distribution within plant tissue. Deciphering these mechanisms enables harnessing the power of microbial communities to promote plant health and foster resilient agriculture in an increasingly challenging environment.

Materials and methods

Strains and culturing conditions

Chitinophaga pinensis 94 was obtained from culture collection of Carrion lab (Carrión et al. 2019) and grown overnight from a 40% glycerol stock in 0.1 × TSB at 25 °C and with agitation (250 rpm). After 16h of growth, 100 µl of overnight culture was diluted into 50 ml 0.1 × TSB and grown for an additional 20h under the same conditions for obtaining long filamentous cells, and 40h for small spherical cells (< 1 µm). Cells were harvested by centrifugation (30 min; 8000 g; 4 °C). Subsequently, cell morphology was checked by light-microscopy (Axion Imager M2; Zeiss) before proceeding with any experiments. All *Bacillus subtilis* strains used in this study (undomesticated *Bacillus subtilis* (NCIB3610); *B. subtilis* DK605 (Δ*mind::TnYLB*); DS1677 (Δ*hag*); DS222 (Δ*motAB*); DK1484 (Δ*espH srfAA::mls*) were cultivated as described before (Muok et al. 2021). *B. subtilis* mini-cell strain (DK605; Δ*mind::TnYLB*) was grown and harvested as previously described (Muok et al. 2021).

Prior to the experiments, the cell morphology of the cultures was assessed microscopically; in the following, the 20 and 40h growth cultures are referred to as filamentous cells and spherical cells, unless otherwise stated. The experiments described below were carried out in triplicates (N = 3) unless otherwise stated.

Trigger assay

Cells of *C. pinensis* after 20h ($OD_{600} = 0.2$) and 40h (OD $OD_{600} = 0.5$) growth in 0.1 × TSB (25 °C; 250 rpm) were harvested by centrifugation (8000 × g; 30 min; 4 °C). Each sample was adjusted to an OD_{600} of 0.2 and 0.5 with fresh medium (0.1 × TSB) and aliquoted with 1 ml. All sample aliquots were then centrifuged (8000 × g; 30 min; 4 °C), the supernatant discarded, and the cell pellets used for the next step.

Preparation of media and culture supernatant for the trigger assay. The supernatant of a 20 and 40h *C. pinensis* culture was extracted by centrifugation (8000 × g; 30 min; 4 °C) and filtration (0.2 µm) for testing whether culture-derived components influence cell size dynamics. These media are referred to below as 'long-filamentous cell media' (LM) and 'small spherical cell media' (SM). Fresh TSB were diluted 1:10 with SM and are referred to as 'SMT' in the following. In addition, phosphate-buffered saline (PBS; pH 7) and fresh 0.1 × TSB medium (FM) were used as reference media for the experiments. The experimental setup is illustrated in Online Resource 8. Aliquots of each sample were resuspended in 1 ml of the respective prepared medium and transferred to 96-well plates (MegaBlock®; 2.2 ml; Sarstedt), which were subsequently incubated at 25 °C and 250 rpm. After 3 and 6h, samples were taken from all wells, treated with Syto9 (1 µM) and fixed with 4% paraformaldehyde. All samples were imaged with an upright fluorescence microscope (Zeiss Axio Imager M2 with AxioCam MRc 5), and the cell length data was determined with ImageJ (Schneider et al. 2012) using the AutoTreshold function. The resulting data were visualized graphically and *p*-values were obtained from a mixed effects regression model, using the logarithm of the cell length to obtain approximate conditional normality and accounting for dependency by including a random effect for "replicate". Mixed models were fit using the lme4 package, and *p*-values were obtained using the lmerTest and emmeans packages lme4 (Bates et al. 2015), lmerTest (Kuznetsova et al. 2017), emmeans (Lenth et al. 2024).

Motility assay

Hitchhiking motility assay

The motility test was performed on 0.1 × TSB agar plates (ø 9 cm) with 0.5% agar for swarming plates and 0.27–0.3% agar for swimming plate assays. First, a new culture of *B. subtilis* and its mutants was prepared from an overnight LB culture and incubated in LB (37 °C; 200 rpm) until an OD_{600} of 0.5 was reached. Subsequently, *C. pinensis* cells were harvested from plate (0.1 × TSA; 25 °C; > 1-week incubation) using a sterile loop and resuspended in 200 µl 0.1 × TSB. The cell morphology of the inoculum was verified by light microscopy prior to the assay and confirmed to consist predominantly of spherical cells. To determine the hitchhiking behaviour, 3 µl of *B. subtilis* cells were transferred to the plate and 3 µl of *C. pinensis* cell suspension was pipetted directly onto the desired inoculation site (either directly on the *B. subtilis* inoculation site or onto a separate site on the plate). For the hitchhiking assay on swimming

plates (0.27–0.3% agar; LP0011; Oxoid), a sterile loop was punctured into each inoculation site after inoculation to promote swimming behaviour inside the agar. The plates were incubated at 25 °C for up to 5 days and imaged on a light box. Experiments were performed in triplicate using Bacto™ Agar (BD) and Agar No. 1 (LP0011; Oxoid). For comparison and control purposes, each condition was also tested on each strain individually.

Surfactin cheating assay

Surfactin cheating assays were performed on 0.1×TSA (0.5% agar) with surfactin from *B. subtilis* (Sigma-Aldrich; St. Luis; Missouri; USA). For the incorporation of surfactant into the medium, 10 ml medium was liquefied by heating in a microwave and 10 µl surfactin (stock: 10 g/L) added after cooling down to room temperature. For the cheating assay in combination with additional potassium, 70 µl of K2HPO4 (1 M) was added to the liquid medium. The medium was then poured into a petri dish (ø 9 cm) and solidified. The topical treatment of media plates was performed by pipetting 10 µl of surfactin (10 g/L) onto the centre of the plate and left under the hood until the surfactin had completely diffused into the agar. The procedure was repeated with 1 g/L surfactin solution. All plates were inoculated with a single colony of *C. pinensis*, taken with a sterile tooth pick from a starting plate (0.1×TSA; 1.5% agar). The plates were incubated at 25 °C for 3 days and imaged on a light box. The experiments were carried out in triplicate. For comparison, media without surfactin and additional potassium were inoculated and treated in the same way.

Fluorescence microscopy

Fluorescence microscopy was performed to evaluate and confirm the successful integration of GFP into the genome of *C. pinensis*. For this purpose, a colony was sampled from a plate, suspended in 3–5 µl PBS on a glass slide, and covered with a coverslip. Microscopy and imaging were carried out using a Zeiss Axio Imager M2 equipped with an AxioCam MRc 5 camera. GFP fluorescence was imaged (Ex 488 nm; Em 510 nm) and analysed in Zeiss Zen software.

Cryo-electron microscopy

Cell pellet obtained from *B. subtilis* mini-cell strain (DK605; Δ*mind::TnYLB*) as described above was resuspended in 12 µl LB. *C. pinensis* spherical cell morphology were harvested with a sterile loop from a 2-week-old 0.1×TSB plate (1.5% agar) and transferred to 200 µl 0.1×TSB medium. From the *C. pinensis* cell suspension, 2 µl were added to the 12 µl *B. subtilis* mini-cells and a 10-nm colloidal gold solution treated with protein A (Cell Microscopy Core, Utrecht University, Utrecht, The Netherlands) was added in a 1/10 dilution. The mixture was gently mixed by pipetting and incubated for 30 min at RT. Subsequently, 3 µl of sample were applied to glow-discharged 200-mesh R2/2 copper grid (Quantifoil Micro tools), pre-blotted for 30s. and then blotted for 1s. in a chamber with 90% humidity and at 20 °C. The grids were plunge frozen in liquid ethane using an automated Leica EM GP system (Leica Microsystems) and then stored in liquid nitrogen. Imaging of the grids was performed with a 120 kV Talos L120C cryo-electron microscope (Thermo Fisher Scientific) at the Netherlands Centre for Electron Nanoscopy (NECEN).

Cryo-electron tomography

The *C. pinensis* cells were prepared as described above and samples were taken after 20h and 40h incubation. The samples were then centrifuged at 3000×g for 5 min. and the cell pellet were resuspended in 20 µl. In addition, a 10-nm solution of colloidal gold treated with protein A (Cell Microscopy Core, Utrecht University, Utrecht, Netherlands) was added in a 1/10 dilution and carefully mixed by pipetting. For vitrification, 3 µl of sample was applied to a glow-discharged grid and plunge frozen as described above. Imaging data were acquired using a TITAN Krios microscope (TFS), equipped with a Gatan K3 Summit direct electron detector and a GATN GIF Quantum energy filter with a slit width of 20 eV. Images were acquired at a nominal magnification of 26,000, which corresponds to a pixel size of 3.28 Å. Tilt series were collected using SerialEM with a bidirectional dose-symmetric tilt scheme (−60°–60; starting from 0°) with a 2° increment. The defocus was set between −8 and −10 µm, and the cumulative exposure per tilt series was 100 e−/A2. Alignment of the

tilt series based on bead tracking and drift correction was performed with IMOD (Xiong et al. 2009) and CTFplotter was used to determine and correct the contrast transfer function (Pham and Parkinson 2011).

Acknowledgements Cryo-EM data were collected at the Netherlands Centre for Electron Nanoscopy (NeCEN) at Leiden University, with technical support from Dr. Wen Yang, Dr. Willem Noteborn, and Dr. Birgit Luef.

Author contributions J.L. designed and conducted the study, performed most experiments, and wrote the manuscript draft. L.Z. contributed to laboratory work and provided input to the Methods section. D.U. supported the interpretation of transcriptomic data. F.R. assisted with statistical analysis and data processing. J.R. contributed to conceptualization and funding acquisition. A.B. and G.P.v.W. supervised the project and provided critical feedback on the manuscript. All authors reviewed and approved the final version.

Funding This work benefited from access to NeCEN, which was funded in part by the Netherlands Electron Microscopy Infrastructure (NEMI), project number 184.034.014 of the National Roadmap for Large-Scale Research Infrastructure of the Dutch Research Council (NWO). J.L. was supported by the OCENW.GROOT.2019.063 and Building Blocks of Life 737.016.00 grants from the Netherlands Organization for Scientific Research (NWO), both awarded to A.B.

Data availability The datasets generated and analysed during this study are available from the corresponding author on request.

Declarations

Conflict of interest The authors declare no conflict of interest.

Ethical approval Not applicable. This study did not involve human participants or animals.

Open Access This article is licensed under a Creative Commons Attribution 4.0 International License, which permits use, sharing, adaptation, distribution and reproduction in any medium or format, as long as you give appropriate credit to the original author(s) and the source, provide a link to the Creative Commons licence, and indicate if changes were made. The images or other third party material in this article are included in the article's Creative Commons licence, unless indicated otherwise in a credit line to the material. If material is not included in the article's Creative Commons licence and your intended use is not permitted by statutory regulation or exceeds the permitted use, you will need to obtain permission directly from the copyright holder. To view a copy of this licence, visit http://creativecommons.org/licenses/by/4.0/.

References

Agarwal S, Hunnicutt DW, McBride MJ (1997) Cloning and characterization of the *Flavobacterium johnsoniae* (*Cytophaga johnsonae*) gliding motility gene, gldA. Proc Natl Acad Sci U S A 94:12139–12144. https://doi.org/10.1073/pnas.94.22.12139

Ariel G, Rabani A, Benisty S, Partridge JD, Harshey RM, Be'er A (2015) Swarming bacteria migrate by Lévy walk. Nat Commun 6:8396. https://doi.org/10.1038/ncomms9396

Bates D, Mächler M, Bolker B, Walker S (2015) Fitting linear mixed-effects models using lme4. J Stat Softw 67:1–48. https://doi.org/10.18637/jss.v067.i01

Briegel A, Ladinsky MS, Oikonomou C et al (2014) Structure of bacterial cytoplasmic chemoreceptor arrays and implications for chemotactic signaling. Elife 3:e02151. https://doi.org/10.7554/eLife.02151

Brinkmann S, Kurz M, Patras MA et al (2022) Genomic and chemical decryption of the Bacteroidetes phylum for its potential to biosynthesize natural products. Microbiol Spectr 10:e0247921. https://doi.org/10.1128/spectrum.02479-21

Campey A, Chait R, Tsaneva-Atanasova K, Pagliara S (2024) Antibiotic resistant bacteria survive treatment by doubling while shrinking. bioRxiv. https://doi.org/10.1101/2024.06.27.601114

Carrión VJ, Perez-Jaramillo J, Cordovez V et al (2019) Pathogen-induced activation of disease-suppressive functions in the endophytic root microbiome. Science 366:606–612. https://doi.org/10.1126/science.aaw9285

Chen S, Bagdasarian M, Kaufman MG, Walker ED (2007) Characterization of strong promoters from an environmental *Flavobacterium hibernum* strain by using a green fluorescent protein-based reporter system. Appl Environ Microbiol 73:1089–1100. https://doi.org/10.1128/AEM.01577-06

Engelhardt IC, Patko D, Liu Y, Mimault M, de las Heras Martinez G, George TS, MacDonald M, Ptashnyk M, Sukhodub T, Stanley-Wall NR, Holden N, Daniell TJ, Dupuy LX (2022) Novel form of collective movement by soil bacteria. ISME J 16:2337–2347. https://doi.org/10.1038/s41396-022-01277-w

Glavina Del Rio T, Abt B, Spring S et al (2010) Complete genome sequence of *Chitinophaga pinensis* type strain (UQM 2034). Stand Genomic Sci 2:87–95. https://doi.org/10.4056/sigs.661199

Hildebrand F, Gossmann TI, Frioux C et al (2021) Dispersal strategies shape persistence and evolution of human gut bacteria. Cell Host Microbe 29:1167-1176.e9. https://doi.org/10.1016/j.chom.2021.05.008

Justice SS, Hunstad DA, Seed PC, Hultgren SJ (2006) Filamentation by *Escherichia coli* subverts innate defenses during urinary tract infection. Proc Natl Acad Sci USA 103:19884–19889. https://doi.org/10.1073/pnas.0606329104

Justice SS, Hunstad DA, Cegelski L, Hultgren SJ (2008) Morphological plasticity as a bacterial survival strategy. Nat Rev Microbiol 6:162–168. https://doi.org/10.1038/nrmicro1820

Kaplan M, Chreifi G, Metskas LA et al (2021) In situ imaging of bacterial outer membrane projections and associated protein complexes using electron cryo-tomography. Elife 10:e73099. https://doi.org/10.7554/eLife.73099

Karasz DC, Weaver AI, Buckley DH, Wilhelm RC (2022) Conditional filamentation as an adaptive trait of bacteria and its ecological significance in soils. Environ Microbiol 24:1–17. https://doi.org/10.1111/1462-2920.15871

Kearns DB (2010) A field guide to bacterial swarming motility. Nat Rev Microbiol 8:634–644. https://doi.org/10.1038/nrmicro2405

Kuznetsova A, Brockhoff PB, Christensen RHB (2017) lmerTest package: tests in linear mixed effects models. J Stat Softw 82:1–26. https://doi.org/10.18637/jss.v082.i13

Lenth RV, Banfai B, Bolker B et al (2024) emmeans: estimated marginal means, aka least-squares means. Comprehensive R Archive Network (CRAN)

Li C, Hurley A, Hu W et al (2021) Social motility of biofilm-like microcolonies in a gliding bacterium. Nat Commun 12:5700. https://doi.org/10.1038/s41467-021-25408-7

Liu H, Li J, Carvalhais LC et al (2021) Evidence for the plant recruitment of beneficial microbes to suppress soil-borne pathogens. New Phytol 229:2873–2885. https://doi.org/10.1111/nph.17057

Liu Y, Zhang H, Wang J et al (2024) Nonpathogenic *Pseudomonas syringae* derivatives and its metabolites trigger the plant "cry for help" response to assemble disease suppressing and growth promoting rhizomicrobiome. Nat Commun 15:1907. https://doi.org/10.1038/s41467-024-46254-3

Lyons NA, Kolter R (2018) A single mutation in rapP induces cheating to prevent cheating in *Bacillus subtilis* by minimizing public good production. Commun Biol 1:133. https://doi.org/10.1038/s42003-018-0136-1

Matsumoto H, Fan X, Wang Y, Kusstatscher P, Duan J, Wu S, Chen S, Qiao K, Ma B, Zhu G, Hashidoko Y, Berg G, Cernava T, Wang M (2021) Bacterial seed endophyte shapes disease resistance in rice. Nat Plants 7:60–72. https://doi.org/10.1038/s41477-020-00826-5

Mattingly AE, Weaver AA, Dimkovikj A, Shrout JD (2018) Assessing travel conditions: environmental and host influences on bacterial surface motility. J Bacteriol 200:e00014-18. https://doi.org/10.1128/JB.00014-18

McBride MJ, Zhu Y (2013) Gliding motility and Por secretion system genes are widespread among members of the phylum Bacteroidetes. J Bacteriol 195:270–278. https://doi.org/10.1128/JB.01962-12

McDonald MD, Owusu-Ansah C, Ellenbogen JB et al (2024) What is microbial dormancy? Trends Microbiol 32:142–150. https://doi.org/10.1016/j.tim.2023.08.006

Meacock OJ, Doostmohammadi A, Foster KR et al (2021) Bacteria solve the problem of crowding by moving slowly. Nat Phys 17:205–210. https://doi.org/10.1038/s41567-020-01070-6

Muok AR, Claessen D, Briegel A (2021) Microbial hitchhiking: how *Streptomyces* spores are transported by motile soil bacteria. ISME J 15:2591–2600. https://doi.org/10.1038/s41396-021-00952-8

Nunan N, Schmidt H, Raynaud X (2020) The ecology of heterogeneity: soil bacterial communities and C dynamics. Philos Trans R Soc Lond B Biol Sci 375:20190249. https://doi.org/10.1098/rstb.2019.0249

Pan X, Raaijmakers JM, Carrión VJ (2023) Importance of Bacteroidetes in host-microbe interactions and ecosystem functioning. Trends Microbiol 31:959–971. https://doi.org/10.1016/j.tim.2023.03.018

Pérez-Jaramillo JE, Carrión VJ, de Hollander M, Raaijmakers JM (2018) The wild side of plant microbiomes. Microbiome 6:143. https://doi.org/10.1186/s40168-018-0519-z

Pham HT, Parkinson JS (2011) Phenol sensing by *Escherichia coli* chemoreceptors: a nonclassical mechanism. J Bacteriol 193:6597–6604. https://doi.org/10.1128/JB.05987-11

Reichenbach H (1992) The order cytophagales. In: Balows A, Trüper HG, Dworkin M et al (eds) The Prokaryotes. Springer, New York, pp 3631–3675

Rizzo MG, De Plano LM, Franco D (2020) Regulation of filamentation by bacteria and its impact on the productivity of compounds in biotechnological processes. Appl Microbiol Biotechnol 104:4631–4642. https://doi.org/10.1007/s00253-020-10590-3

Rolfe SA, Griffiths J, Ton J (2019) Crying out for help with root exudates: adaptive mechanisms by which stressed plants assemble health-promoting soil microbiomes. Curr Opin Microbiol 49:73–82. https://doi.org/10.1016/j.mib.2019.10.003

Salas-González I, Reyt G, Flis P et al (2021) Coordination between microbiota and root endodermis supports plant mineral nutrient homeostasis. Science 371:eabd0695. https://doi.org/10.1126/science.abd0695

Samad T, Billings N, Birjiniuk A et al (2017) Swimming bacteria promote dispersal of non-motile staphylococcal species. ISME J 11:1933–1937. https://doi.org/10.1038/ismej.2017.23

Sangkhobol V, Skerman VBD (1981) *Chitinophaga*, a new genus of chitinolytic myxobacteria. Int J Syst Evol Microbiol 31:285–293. https://doi.org/10.1099/00207713-31-3-285

Santamaria G, Liao C, Lindberg C et al (2022) Evolution and regulation of microbial secondary metabolism. Elife 11:e76119. https://doi.org/10.7554/eLife.76119

Schneider CA, Rasband WS, Eliceiri KW (2012) NIH image to imageJ: 25 years of image analysis. Nat Methods 9(7):671–675. https://doi.org/10.1038/NMETH.2089

Seymour JR, Brumley DR, Stocker R, Raina JB (2024) Swimming towards each other: the role of chemotaxis in bacterial interactions. Trends Microbiol 32:640–649. https://doi.org/10.1016/j.tim.2023.12.008

Shah V, Zhao X, Lundeen RA et al (2019) Morphological plasticity in a sulfur-oxidizing marine bacterium from the SUP05 Clade enhances dark carbon fixation. Mbio 10:e00216-e219. https://doi.org/10.1128/mBio.00216-19

Shrivastava A, Berg HC (2015) Towards a model for *Flavobacterium* gliding. Curr Opin Microbiol 28:93–97. https://doi.org/10.1016/j.mib.2015.07.018

Sly LI, Taghavi M, Fegan M (1999) Phylogenetic position of *Chitinophaga pinensis* in the *Flexibacter-Bacteroides-Cytophaga* phylum. Int J Syst Bacteriol 49:479–481. https://doi.org/10.1099/00207713-49-2-479

Spooren J, van Bentum S, Thomashow LS et al (2024) Plant-driven assembly of disease-suppressive soil microbiomes.

Annu Rev Phytopathol 62:1–30. https://doi.org/10.1146/annurev-phyto-021622-100127

Sudo SZ, Dworkin M (1969) Resistance of vegetative cells and microcysts of *Myxococcus xanthus*. J Bacteriol 98:883–887. https://doi.org/10.1128/jb.98.3.883-887.1969

Tran TD, Ali MA, Lee D et al (2022) Bacterial filamentation as a mechanism for cell-to-cell spread within an animal host. Nat Commun 13:693. https://doi.org/10.1038/s41467-022-28297-6

Trivedi P, Leach JE, Tringe SG et al (2020) Plant-microbiome interactions: from community assembly to plant health. Nat Rev Microbiol 18:607–621. https://doi.org/10.1038/s41579-020-0412-1

Ultee E, Ramijan K, Dame RT et al (2019) Stress-induced adaptive morphogenesis in bacteria. Adv Microb Physiol 74:97–141. https://doi.org/10.1016/bs.ampbs.2019.02.001

Vandenkoornhuyse P, Quaiser A, Duhamel M et al (2015) The importance of the microbiome of the plant holobiont. New Phytol 206:1196–1206. https://doi.org/10.1111/nph.13312

Vives-Peris V, de Ollas C, Gómez-Cadenas A, Pérez-Clemente RM (2020) Root exudates: from plant to rhizosphere and beyond. Plant Cell Rep 39:3–17. https://doi.org/10.1007/s00299-019-02447-5

Weart RB, Lee AH, Chien AC et al (2007) A metabolic sensor governing cell size in bacteria. Cell 130:335–347. https://doi.org/10.1016/j.cell.2007.05.043

Wucher BR, Bartlett TM, Hoyos M et al (2019) *Vibrio cholerae* filamentation promotes chitin surface attachment at the expense of competition in biofilms. Proc Natl Acad Sci USA 116:14216–14221. https://doi.org/10.1073/pnas.1819016116

Xavier JB (2011) Social interaction in synthetic and natural microbial communities. Mol Syst Biol 7:483. https://doi.org/10.1038/msb.2011.16

Xavier JB, Kim W, Foster KR (2011) A molecular mechanism that stabilizes cooperative secretions in *Pseudomonas aeruginosa*. Mol Microbiol 79:166–179. https://doi.org/10.1111/j.1365-2958.2010.07436.x

Xiong Q, Morphew MK, Schwartz CL et al (2009) CTF determination and correction for low dose tomographic tilt series. J Struct Biol 168:378–387. https://doi.org/10.1016/j.jsb.2009.08.016

Yang W, Briegel A (2020) Diversity of bacterial chemosensory arrays. Trends Microbiol 28:68–80. https://doi.org/10.1016/j.tim.2019.08.002

Publisher's Note Springer Nature remains neutral with regard to jurisdictional claims in published maps and institutional affiliations.